ARTICLES

Quantum Mechanical Calculations for the $H_2O + h\nu \rightarrow O(^1D) + H_2$ Photodissociation Process

Rob van Harrevelt*

Institute for Molecules and Materials, Radboud University Nijmegen, Toernooiveld 1, 6525 ED Nijmegen, the Netherlands

Marc C. van Hemert

Leiden Institute of Chemistry, Leiden University, P.O. Box 9502, 2300 RA Leiden, The Netherlands

Received: December 18, 2007

Quantum mechanical wavepacket calculations for the photodissociation of water in the second absorption band are presented. Using $O + H_2$ Jacobi coordinates, partial cross sections for the $O(^1D) + H_2$ channel are calculated for different initial rotational states. Conical intersection and Renner−Teller effects are included. The branching ratios for the four accessible dissociation channels at 121.6 nm are in good agreement with experiment (*J. Chem. Phys.* **1982**, *77*, 2432). The calculations predict significant rotational and vibrational excitation of the H_2 fragments. Photodissociation of ortho and para water produces predominantly, but not exclusively, ortho and para H_2 fragments, respectively.

I. Introduction

For photodissociation of water in the second absorption band, various fragmentation pathways are possible. The following dissociation channels have been identified experimentally[1−3] for excitation with Lyman α radiation:

$$H_2O + h\nu \rightarrow OH(A^2\Sigma) + H \quad \text{(a)}$$

$$\rightarrow O(^1D) + H_2(X^1\Sigma_g^+) \quad \text{(b)}$$

$$\rightarrow OH(X^2\Pi) + H \quad \text{(c)}$$

$$\rightarrow O(^3P) + H + H \quad \text{(d)}$$

The OH fragments have been studied in detail, both experimentally[2−8] and theoretically.[9] In contrast, the H_2 fragments have never been observed directly nor studied theoretically. Consequently, the vibrational and rotational distributions are unknown. Only the total branching ratio for the $O(^1D) + H_2$ channel has been measured in the old experiment of Slanger and Black.[1] The branching ratio has also been calculated in a classical trajectory study.[10]

The $H_2O + h\nu \rightarrow O(^1D) + H_2(X^1\Sigma_g^+)$ channel plays an important role in cometary atmospheres. The photodissociation of water is the primary source of H_2[11] in comets. The analysis of H_2 emission lines from comets suggest that the H_2 fragments are highly vibrationally and rotationally excited. Thus, for a good understanding of the cometary atmospheres, it is desirable to have a detailed picture of the $O + H_2$ channel. The aim of this work is to calculate the cross sections for the $O + H_2$ channel based on quantum mechanical calculations. The vibrational and rotational distributions of the H_2 fragment are also presented.

The energy of Lyman α radiation lies in the second absorption band of water, a broad continuum band arising from the $\tilde{X}^1A_1 \rightarrow \tilde{B}^1A_1$ transition. At the high-energy part of the absorption band, around Lyman α, the spectrum also shows some sharper peaks due to excitation to the $\tilde{C}^1B_1$ and $\tilde{D}^1A_1$ states. The latter states are bound states and predissociated by the dissociative $\tilde{B}^1A_1$ state. To obtain a cross section for the $O + H_2$ channel, it is therefore reasonable to study fragmentation dynamics starting from the $\tilde{B}^1A_1$ state.

Because of conical intersection and Renner−Teller effects, the $\tilde{B}^1A_1$ state is strongly coupled with the $\tilde{X}^1A_1$ and $\tilde{A}^1B_1$ states. Channels c and d correlate with the latter two states. The present study employs the Dobbyn−Knowles[12] potential energy surfaces for the three coupled electronic states in a diabatic representation.

The article is organized as follows. Section II describes the theory for triatomic molecules including the Renner−Teller effect, based on a treatise by Petrongolo.[13] The section also describes in detail the different possible coordinate systems, which is an important issue in this article, since different coordinate systems are employed to obtain cross sections for the various dissociation channels. Section III discusses the potential energy energy surfaces, and section IV describes details of the calculations. Section V presents the results of the calculations: cross sections for the $O(^1D) + H_2$ channel and rovibrational distributions of the H_2 fragments. Section VI concludes and summarizes the paper.

II. Theory

II.1. Jacobi Coordinates. The present work employs different Jacobi coordinates. In general, Jacobi coordinates for triatomic molecules can be defined as follows. The three atoms are labeled

10.1021/jp711857w CCC: $40.75
Published on Web 03/14/2008

TABLE 1. Roto-Electronic Basis Functions $Y^{JM\eta}_{\Omega\Lambda K}$ ($\Omega \geq 0$). η is Related to the Total Parity p According to $p = \eta(-1)^J$. The Complex Wavefunctions $|\Lambda^{\pm}\rangle$ are Defined as $|\Lambda^{\pm}\rangle \equiv (|\Lambda'\rangle \pm i|\Lambda''\rangle)/\sqrt{2}$ for $\Lambda > 0$. Thus, $\hat{L}_z|\Lambda^{\pm}\rangle = \pm\Lambda|\Lambda^{\pm}\rangle$

$Y^{JM\eta}_{\Omega 0\Omega}$	$\Theta^{JM\pm\eta}_{\Omega}\,\|\Sigma^{\pm}\rangle$	$(\Lambda = 0)$
$Y^{JM1}_{0\Lambda\Lambda}$	$\Theta^{JM1}_{0}\,\|\Lambda'\rangle$	$(\Lambda > 0)$
$Y^{JM-1}_{0\Lambda\Lambda}$	$-\mathrm{i}\,\Theta^{JM1}_{0}\,\|\Lambda''\rangle$	$(\Lambda > 0)$
$Y^{JM\eta}_{\Omega\Lambda\|\Omega\pm\Lambda\|}$	$\sqrt{(2J+1)/8\pi^2}\,\sqrt{1/2}\,\{(D^J_{M\Omega})^*\,\|\Lambda^{\mp}\rangle + \eta(-1)^{\Omega}\,(D^J_{M\Omega})^*\,\|\Lambda^{\pm}\rangle\}$	$(\Lambda > 0, \Omega > 0)$

arbitrarily as A, B, and C, which positions given by the three vectors $\mathbf{r_A}$, $\mathbf{r_B}$, and $\mathbf{r_C}$. After separating out the center of mass, the system can be described by two vectors **r** and **R**. The vector **r** connects atom B with atom A: $\mathbf{r} \equiv \mathbf{r_B} - \mathbf{r_A}$, and **R** connects the center of mass of the pair AB ($\mathbf{r^{CM}_{AB}}$) with atom C: $\mathbf{R} \equiv \mathbf{r_C} - \mathbf{r^{CM}_{AB}}$.

The lengths of the vectors **r** and **R**, r and R respectively, and the angle between the two vectors, γ, form the internal coordinates. The rotational motion is described by the three Euler angles ϕ, θ, and χ,[14] collectively referred to as ω. The Euler angles describe the orientation of a body-fixed frame with respect to a space fixed frame. There are several approaches to define a body-fixed frame. In combination with Jacobi coordinate systems, two possible choices are r and R embedding, in which the **r** and **R** vectors are chosen as body-fixed z-axes, respectively. The coordinate system will be labeled AB + C(R) for R-embedding, and AB + C(r) for r-embedding. For example, for water four Jacobi coordinate systems can be defined: OH + H(R), OH + H(r), O + H_2(R), and O + H_2(r).

Expressions of the nuclear kinetic energy operator in the Jacobi coordinate systems are given by Tennyson and Sutcliffe[15] and Petrongolo.[13]

II.2. Roto-Electronic Basis Functions. The various degrees of freedom of a molecule can be divided in three groups: internal coordinates (r, R, γ), the Euler angles ω, and the electronic degrees of freedom. The rotational and electronic degrees of freedom are described using basis functions. The rotational basis functions are the parity-adapted symmetric top eigenfunctions[14]

$$\Theta^{JM\epsilon}_{\Omega}(\omega) = \sqrt{\frac{2J+1}{8\pi^2}}\frac{1}{\sqrt{2(1+\delta_{\Omega 0})}}\{(D^J_{M\Omega}(\omega))^* + \epsilon(-1)^{\Omega}(D^J_{M\Omega}(\omega))^*\} \quad (1)$$

where $D^J_{M\Omega}(\omega)$ is a rotation matrix, J is the total angular momentum, Ω and M the projections of $\hat{\mathbf{J}}$ on the body-fixed z-axis and the space-fixed Z-axis, and $\epsilon = \pm 1$. The parity of the function $\Theta^{JM\epsilon}_{\Omega}(\omega)$ is equal to $\epsilon(-1)^J$.

The total wavefunction is expanded in terms of these rotational basis functions and a set of electronic wavefunctions $|\psi^{\mathrm{el}}_n\rangle$ (n is an electronic state index):

$$\Psi^{JMp} = \sum_{\Omega n}\chi_{\Omega n}(r, R, \gamma)\Theta^{JM\epsilon_n}_{\Omega}(\omega)|\psi^{\mathrm{el}}_n\rangle \quad (2)$$

In general, only J, M, and p (the total parity) are good quantum numbers. (For a discussion of symmetry in AB_2 type molecules, see section II.5). The parameter ϵ_n depends on the total parity p and on the symmetry of the electronic wavefunction $|\psi^{\mathrm{el}}_n\rangle$: $\epsilon_n = p(-1)^J$ for A′ states, and $\epsilon_n = -p(-1)^J$ for A″ states.

The kinetic energy operator acts on all nuclear degrees of freedom and therefore results in a coupling between the different rotational and electronic states. The kinetic energy operator has the form

$$\hat{T} = \hat{T}^{\mathrm{vib}} + \hat{T}^{\mathrm{rot}} \quad (3)$$

where the term $\hat{T}^{\mathrm{vib}}$ only depends on the internal coordinates (r, R, and γ), while the rotational kinetic energy operator $\hat{T}^{\mathrm{rot}}$ depends on all coordinates. In the expansion, eq 2, the electronic states $|\psi^{\mathrm{el}}_n\rangle$ are assumed to be diabatic electronic states. Matrix elements of $\hat{T}^{\mathrm{vib}}$ between diabatic electronic states are neglected. However, the $\hat{T}^{\mathrm{rot}}$ couples the two electronic states that correlate to a doubly degenerate electronic state at linear geometries (e.g., a Π or Δ state).[13]

The two electronic states that become degenerate at linear geometries will be labeled as $|\Lambda'\rangle$ and $|\Lambda''\rangle$, where Λ is 1, 2, ... for Π, Δ, ... states. The C_s point group symmetry species of the $|\Lambda'\rangle$ and $\Lambda''\rangle$ states are A′ and A″, respectively. The coupling between the $|\Lambda'\rangle$ and $|\Lambda''\rangle$ arises from the $\hat{R}_z$ term in the nuclear kinetic energy operator.[13] $\hat{R}_z$, the z component of the nuclear angular momentum, is equal to $\hat{J}_z - \hat{L}_z$, where $\hat{J}_z$ and $\hat{L}_z$ are the z-components of the total and electronic angular momentum, respectively. The spin angular momentum has been ignored. It is the $\hat{J}_z\hat{L}_z$ term in the Hamiltonian that mixes the $|\Lambda'\rangle$ and $|\Lambda''\rangle$ states. The resulting coupling is singular for linear geometries ($\gamma = 0$ or $\gamma = 180°$). This effect is called the Renner−Teller effect.

At linear geometries and for r embedding[2,13]

$$\langle\Lambda'|\hat{L}_z|\Lambda''\rangle = -i\Lambda \quad (r - \text{embedding}) \quad (4)$$

In the following, we neglect the coordinate dependence of $\langle\Lambda'|\hat{L}_z|\Lambda''\rangle$, and we thereby assume that eq 4 also holds for nonlinear geometries. It is then possible to construct roto-electronic basis functions that are eigenfunctions of the rotational kinetic energy operator $\hat{T}^{\mathrm{rot}}$. The functions $Y^{JM\eta}_{\Omega\Lambda K}$, defined in Table 1, are eigenfunctions of $(\hat{J}_z - \hat{L}_z)^2$ with eigenvalue K^2, assuming that eq 4 is valid. When the wavefunction is expanded in these roto-electronic basis functions, then the singularities in the kinetic energy operator can be removed.[13] The electronic basis function used in Table 1 include, besides the $|\Lambda'\rangle$ and $|\Lambda''\rangle$ states defined above, also a $|\Sigma^{\pm}\rangle$ state. The $|\Sigma^{+}\rangle$ and $|\Sigma^{-}\rangle$ states correlate to a nondegenerate electronic state at linear geometries, and transforms as A′ or A″ respectively. For linear geometries, matrix elements of $\hat{L}_z$ between a $|\Sigma^{\pm}\rangle$ state and other electronic states are zero. We will again assume that this also hold for nonlinear geometries.

In the roto-electronic basis, off-diagonal matrix elements of the rotational terms in the kinetic energy operator are zero. However, $Y^{JM\eta}_{\Omega\Lambda|\Omega-\Lambda|}$ and $Y^{JM\eta}_{\Omega\Lambda\Omega+\Lambda}$ are coupled due the electronic Hamiltonian $\hat{H}^{\mathrm{el}}$:

$$\langle Y^{JM\eta}_{\Omega\Lambda|\Omega-\Lambda|}|\hat{H}^{el}|Y^{JM\eta}_{\Omega\Lambda\Omega+\Lambda}\rangle = (\langle\Lambda'|\hat{H}^{\mathrm{el}}|\Lambda'\rangle - \langle\Lambda''|\hat{H}^{el}|\Lambda''\rangle)/2 \quad (5)$$

which is nonzero for bent geometries.

II.3. Matrix Elements of the Kinetic Energy Operator. For the evaluation of the kinetic energy operator on the wavefunction, it is useful to expand the wavefunction in terms of coupled roto-electronic basis functions discussed before:

$$\Psi^{JMp} = \sum_{\Omega\Lambda K} \chi_{\Omega\Lambda K}(r, R, \gamma) Y^{JM\eta}_{\Omega\Lambda K} \tag{6}$$

where $|\Omega - \Lambda| \le K \le \Omega + \Lambda$ and $\eta = p(-1)^J$. The vibrational amplitudes $\chi_{\Omega\Lambda K}(r, R, \gamma)$ are further expanded in normalized associated Legendre polynomials $\tilde{P}_{jK}(\gamma)$:

$$\chi_{\Omega\Lambda K}(r, R, \gamma) = \sum_j f_j^{\Omega\Lambda K}(r, R) \tilde{P}_{jK}(\gamma) \tag{7}$$

The advantage of the expansions eqs 6 and 7 is that matrix elements of the kinetic operator have no singularities. The matrix elements of the various terms in the kinetic energy operator expressions are given in ref 9. Following Petrongolo,[13] the $\hat{R}_z$ terms are replaced by $\hat{J}_z - \hat{L}_z$, while the $\hat{L}^{\pm}$ terms are neglected.

The expression of the matrix elements of the Coriolis operator in ref 9 contains a small mistake. Therefore, we give here the correct expressions. The Coriolis operator is given by[13]

$$\hat{T}^{\text{Corio}} = \frac{1}{2\mu_\rho \rho^2} \left\{ \hat{R}^+ \left(\hat{R}_z \cot\gamma + \frac{\partial}{\partial\gamma} \right) + \hat{R}^- \left(\hat{R}_z \cot\gamma - \frac{\partial}{\partial\gamma} \right) \right\} \tag{8}$$

where ρ is r or R for r- and R- embedding, respectively, and μ_ρ is the corresponding reduced mass. The matrix elements of the Coriolis operator can be derived using the relations[14]

$$\hat{J}^{\pm} D^J_{M\Omega}(\omega)^* = \lambda^{\mp}(J,\Omega) D^J_{M\Omega\mp1}(\omega)^* \tag{9}$$

and

$$\left(K \cot\gamma \pm \frac{\partial}{\partial\gamma} \right) \tilde{P}_{jK}(\gamma) = -\lambda^{\mp}(J,\Omega) \tilde{P}_{jK\mp1}(\gamma) \tag{10}$$

where

$$\lambda^{\pm}(l,m) = \sqrt{l(l+1) - m(m \pm 1)} \tag{11}$$

The Coriolis operator couples states with $|\Delta\Omega| = |\Delta K| = 1$. For $\Lambda \le 1$, the matrix elements of the Coriolis operator are given by

$$\langle Y^{JM\eta}_{|\Omega\pm1|\Lambda|K\pm1|} \tilde{P}_{j|K\pm1|}(\gamma) | \hat{T}^{\text{corio}} | \tilde{P}_{jK}(\gamma) Y^{JM\eta}_{\Omega\Lambda K} \rangle = \frac{-\lambda^{\pm}(J,\Omega)\lambda^{\pm}(J,K) f^{\pm}_{\eta\Omega\Lambda K}}{2\mu_\rho \rho^2} \tag{12}$$

The factor $f^{\pm}_{\eta\Omega\Lambda K} = 1$, with the following exceptions: $f^{+}_{1000} = \sqrt{2}$, $f^{-}_{1101} = \sqrt{2}$, $f^{-}_{1000} = 0$, $f^{-}_{-1101} = 0$, $f^{-}_{1110} = -1$, and $f^{-}_{1011} = -1$. (In ref 9, f^{-}_{1110} and f^{-}_{1011} were incorrectly equal to 1). The corresponding expressions for $\Lambda > 1$ are more complex. This case is not relevant to the present study, where only Σ and Π states play a role.

II.4. Transformation between Embeddings. Suppose that we want to describe dissociation process ABC → AB + C. In order to obtain rovibrational distributions of the AB fragments, it is convenient if the wavefunction is represented using an AB + C(R) coordinate system. In that case, the index j in the expansion in eq 7 represents the rotational quantum number of the diatomic fragment.

However, in some cases it is advantageous to use r embedding in the wavepacket propagation. For example, for r-embedding coordinate systems, we can employ eq 4 to construct roto-electronic basis functions that are eigenfunctions of $(\hat{J}_z - \hat{L}_z)^2$. In r embedding, j represents the orbital angular momentum of the C atom, relative to the center of mass of AB. Fortunately, the wavepackets can be easily transformed from an r embedding to an R embedding representation.

In the transformation, we employ the uncoupled representation of electronic and rotational basis functions (eq 2). The vibrational wavefunctions for r and R embedding are then related according to (see Zare[14]):

$$\chi^R_{\Omega'}(r, R, \gamma) = \sum_\Omega M_{\Omega\Omega'}(\gamma) \chi^r_\Omega(r, R, \gamma) \tag{13}$$

where

$$M_{\Omega\Omega'}(\gamma) = N_{\Omega\Omega'} \{ d^J_{\Omega\Omega'}(\gamma) + \epsilon(-1)^\Omega d^J_{-\Omega\Omega'}(\gamma) \} \tag{14}$$

$d^J_{\Omega\Omega'}(\gamma)$ is a rotation matrix element, and $N_{\Omega\Omega'} = 1$ if both Ω and Ω' are nonzero, $N_{\Omega\Omega'} = 1/\sqrt{2}$ if one of Ω and Ω' is zero, and $N_{\Omega\Omega'} = {}^1/_2$ if both Ω and Ω' are zero.

III. Potential Energy Surfaces

Three electronic states are involved in the dissociation dynamics of water in the second absorption band: the $\tilde{X}^1A'$, $\tilde{A}^1A''$, and the $\tilde{B}^1A'$ states. The relevant potential energy surfaces, obtained by Dobbyn and Knowles, are given in a diabatic representation.[12] Using the convention discussed in section II 2, these diabatic states can be written as $|\Sigma\rangle$, $|\Pi'\rangle$, and $|\Pi''\rangle$.

The matrix of the electronic Hamiltonian $\hat{H}_{\text{el}}$ in the basis ($|\Sigma\rangle$ $|\Pi'\rangle$ $|\Pi''\rangle$) has the following form:

$$\begin{pmatrix} V_\Sigma & V_{\Sigma\Pi} & 0 \\ V_{\Sigma\Pi} & V_{\Pi'} & 0 \\ 0 & 0 & V_{\Pi''} \end{pmatrix} \tag{15}$$

Diagonalization of the (2 × 2) matrix involving Σ and Π' yield the adiabatic potential energies for the $\tilde{X}^1A'$ and $\tilde{B}^1A'$ states. $V_{\Pi''}$ is the adiabatic potential energy of the $\tilde{A}^1A''$ state. The adiabatic potentials $\tilde{X}^1A'$, $\tilde{B}^1A'$, and $\tilde{A}^1A''$ states correlate with the $\tilde{X}^1A_1$, $\tilde{B}^1A_1$, and $\tilde{A}^1B_1$ states at C_{2v} geometries, respectively. At linear geometries, $V_{\Sigma\Pi} = 0$ and $V_{\Pi'} = V_{\Pi''}$.

The transition dipole moment surfaces are taken from ref 16.

IV. Details of the Calculations

The photodissociation cross sections are calculated using a time-dependent wavepacket approach. For the representation of the wavepacket, we employ coupled roto-electronic basis functions as in eq 6. The time-dependent vibrational amplitudes $\chi_{\Omega LK}(r, R, \gamma; t)$ are represented using a three-dimensional grid. Further details are given in ref 9.

All numerical parameters are chosen on the basis of extensive sets of convergence tests. The results are converged within a few percent. Table 2 gives details about the grids employed to represent the vibrational amplitudes. For r and R we use equidistant grid points (Fourier grid), and for γ the Legendre DVR. For H_2 + O coordinates, the potential energy surface is an even function of cos γ. We therefore used a symmetry-adapted Legendre DVR with grid points between 0 and 90°. The total propagation time is 960 fs.

To calculate branching ratios for the different fragmentation channels, we employ two different coordinate systems: OH + H(r) for the OH + H channels, and O + H_2(r) for the O(^{1}D) + H_2 channel. Using r embedding facilitates the treatment of the electronic angular momentum terms in the Hamiltonian, since

$$\langle \Pi' | L_z | \Pi'' \rangle = -i \tag{16}$$

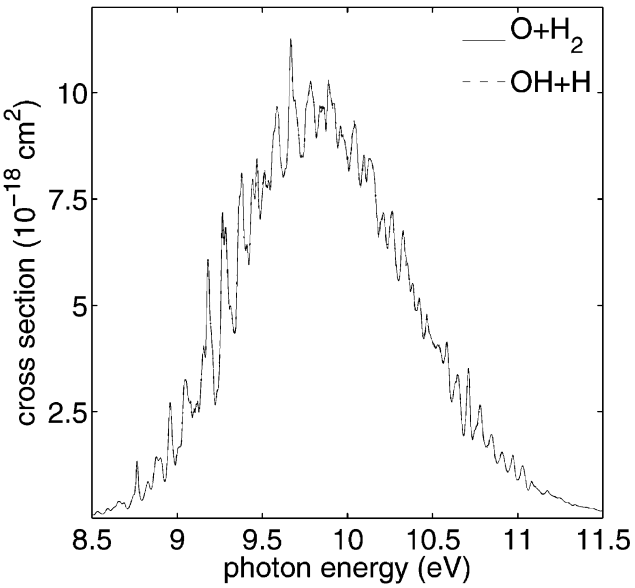

Figure 1. Absorption cross section as a function of the photon energy. The initial rotational state $J''_{K_a''K_c''} = 0_{00}$. Shown are results obtained using different coordinate systems: OH + H and O + H_2 Jacobi coordinates, both employing the *r*-embedding scheme.

TABLE 2. Details of the Grids Employed in Wavepacket Propagation, for Calculations Using O + H_2(*r*) and OH + H(*r*) Coordinate Systems, Where N_i Stands for the Number of Grid Points for Coordinate *i*

	O + H_2	OH + H
range *R*	0−12 bohr	1−16 bohr
N_R	116	176
range *r*	0.3−14 bohr	1−16 bohr
N_r	192	176
range γ	0−90°	0−180°
N_γ	48	120

for linear geometries if OH + H(*r*)[2] and O + H_2(*r*)[13] coordinate systems are used. In order to use the treatment of section II, it is necessary to make the approximation that eq 16 also holds for nonlinear geometries. However, it is impossible that $\langle\Pi'|L_z|\Pi''\rangle$ is constant for both OH + H(*r*) and O + H_2(*r*) coordinate systems. If $\langle\Pi'|L_z|\Pi''\rangle = -i$ for OH + H(*r*) coordinates, as in previous work,[2,9] then $\langle\Pi'|L_z|\Pi''\rangle = -i\cos\beta$ for O + H_2(*r*) coordinates, where β is the angle between the **r** vectors for the O + H_2 and OH + H coordinate systems.

Nevertheless, in this work we use the approximation that the matrix element of $\hat{L}_z$ is constant for both coordinate systems. This means that calculations using different coordinate systems (OH + H(*r*) and O + H_2(*r*)) are not strictly equivalent. The effect of the different approximations is probably small, because the Renner−Teller coupling is only important near linear geometries, where eq 16 is a good approximation for both coordinate systems.

V. Results and Discussion

V.1. Cross sections for the O + H_2 Channel. In the present work, two coordinate systems are employed to obtain partial cross sections for different channels: OH + H(*r*) and O + H_2-(*r*). Ideally, the absorption spectrum should be independent of the coordinate system employed. However, due to the approximations made in the electronic angular momentum terms in the Hamiltonian (see section IV), the calculations using different coordinate systems are not strictly equivalent. Thus, the spectra obtained with two coordinate systems do not have to be exactly the same. However, Figure 1 shows that the differences are quite small: they are hardly visible in this figure. This implies that it is reasonable to combine the results of calculations employing different coordinate systems to obtain branching ratios. If the electronic angular momentum terms were neglected, then the two coordinate systems should give identical results. We checked that this was indeed the case.

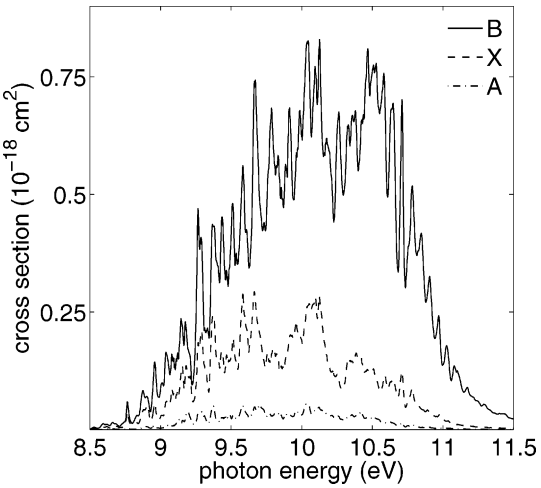

Figure 2. Partial cross section for the O(^{1}D) + H_2 channel, divided into the contributions of the different adiabatic electronic states, as a function of the photon energy. The intitial rotational state is 0_{00}.

The comparison of the calculated cross section with experiment is discussed in detail in ref 17.

Figure 2 presents the cross section for the formation of H_2 fragments for each adiabatic electronic state. The majority of H_2 fragments is formed on the $\tilde{B}$ state surface, a small part on the ground state surface, and a minute part on the $\tilde{A}$ surface. The H_2 fragments can be formed on the ground state surface because of the conical intersection of the $\tilde{B}$ and $\tilde{X}$ energy surfaces. However, the ground state favors dissociation to OH + H, which explains the small contribution of the $\tilde{X}$ state to the O(^1D) + H_2 channel. The fragments produced on the $\tilde{A}$ state result from the roto-electronic coupling between the Π' and Π'' states for $\Omega > 0$ (the Renner−Teller effect). The water molecules are initially in their rotational ground state ($J''_{K_a''K_c''} = 0_{00}$)). The selection rules states that the rotational angular momentum in the excited state, *J*, is then equal to one. ($J = 1$). Since the water molecules are slowly rotating, the Renner−Teller coupling is small.

V.2. Branching Ratios: Comparison with Experiment. The branching ratios for different fragmentation channels are presented in Figure 3. The branching ratios are obtained by summing over all rovibrational product states of the fragment with an energy below the dissociation energy. For the H_2 and OH(A) fragments, the dissociation energy is higher than the available energy. However, for the OH(X) fragment, the dissociation energy is only 9.94 eV. The branching ratio for the OH(X) + H channel therefore does not include metastable excited states with energies above the dissociation energy. Because of rotational barriers, these state may have a nonzero lifetime. The branching ratio for the O(^{3}P) + 2H channel is obtained by subtracting the total cross sections for the OH + H and O + H_2 channels from the absorption cross section. Because of small numerical uncertainties, the branching ratio is not exactly zero below the threshold for three-body dissociation energy, at 9.36 eV. The present results are in reasonable agreement with quasi-classical trajectory results.[10]

Table 3 gives the branching ratios for a photon energy of 10.2 eV (Ly α) and compares the results with experimental

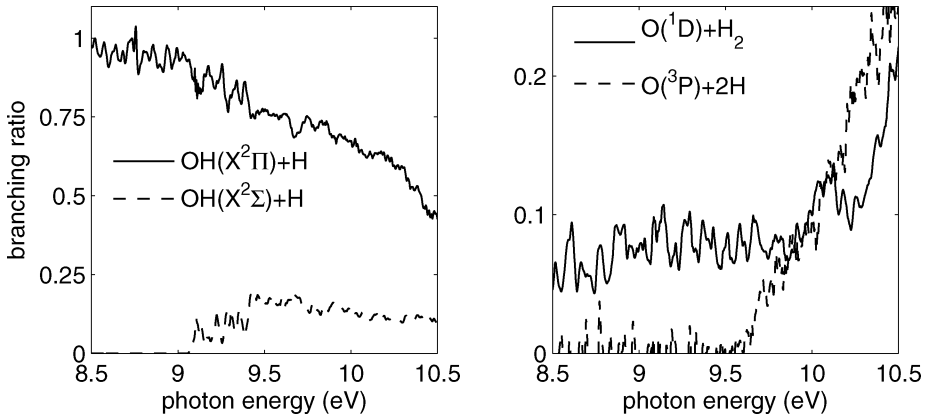

Figure 3. Branching ratios: OH + H channels (panel a) and the non-OH channels (panel b). The initial rotational state is 0_{00}.

TABLE 3. Branching Ratios and H Product Ratios for Ly α Photodissociation[a]

	branching ratio	exp. [1]	H product ratio	exp 6
$OH(X^2\Pi) + H$	0.61		0.57	0.54
$OH(A^2\Sigma) + H$	0.11		0.10	0.11
OH + H (total)	0.72	0.78	0.67	0.65
$O(^3P) + 2H$	0.17	0.12	0.33	0.35
$O(^1D) + H_2$	0.10	0.10	0	0

[a] The H product ratio is the relative contribution of a particular channel to the total number of hydrogen atom fragments. The initial rotational state is the 0_{00} state.

values. The branching ratios have been measured a long time ago by Slanger and Black.[1] Their branching ratio for the $O(^1D) + H_2$ channel agrees well with the present theoretical result. However, the same experiment gives a significantly smaller branching ratio for the three-body dissociation channel $O(^3P) + 2H$. More recent experiments have focused on the H-producing channels, using the Rydberg tagging time-of-flight approach.[2,6] The H product ratios obtained in the most recent experiments[6] agree quite well with the present theoretical results (see Table 3). Harich et al. found somewhat less OH(X) + H, probably because they only included vibrational levels up to $v = 9$ in their analysis. The present calculations, however, show that all vibrational levels up to $v_{max} = 17$ are populated.

The experimental branching ratio for the three-body dissociation channel is subject to significant error.[6] In an older study,[2] a smaller H product ratio was found (0.22%) for the three-body dissociation. On the other hand, a recent laser-induced fluorescence study[18] found an H atom quantum yield of 1.39. This implies that the branching ratio for the three-body dissociation is at least 0.39, which is much larger than other experimental or theoretical results. In summary, experimental studies do not provide a consistent picture concerning the branching ratios. Nevertheless, it is clear that OH(X) + H is the dominant channel, and that all four channels (a)-(d) are significant.

The branching ratios presented in Figure 3 and Table 3 are based on calculations for the rotational ground state. The experimental branching ratios[1] are for room temperature, while the measured H product ratios[6] are for cold water ($T \approx 10K$). The question arises whether it is reasonable to compare the branching ratios for water at different temperatures. After all, the Renner−Teller coupling between the Π′ and Π″ states increases with the rotational excitation. Since the Π″ states favors dissociation to OH + H, one would expect that the branching ratio for the $O(^1D) + H_2$ channel would decrease with rotational excitation of the parent molecule.

Figure 4 compares the $O + H_2$ branching ratio for two rotational states: 0_{00} and the 4_{23}. The latter is a rotational state

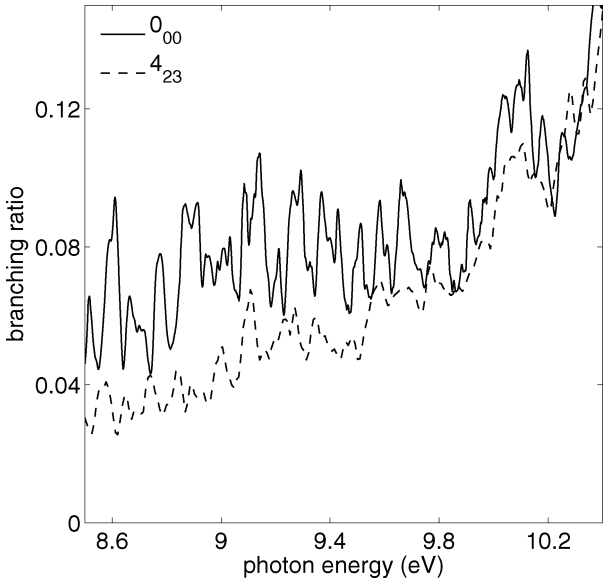

Figure 4. Branching ratio for the $O(^1D) + H_2$ channel for two different initial rotational states.

typically populated at room temperature. For the rotationally excited state, the branching ratio is smaller than for ground state, as expected. However, with increasing energy, the difference diminishes. At Lyman α (10.2 eV), the difference is negligible. This suggests that the branching ratios for Ly α photodissociation are not sensitive to the temperature. Calculations for other rotational states show the same trend.

V.3. Rovibrational Distributions of H_2 Fragments. In previous publications,[2−8] the rovibrational distributions of the OH(X) and OH(A) fragments have been discussed extensively. Rovibrational distributions of the H_2 fragments have not yet been studied before, either experimentally or theoretically. This section discusses the results of the present calculations.

The H_2 fragments are highly vibrationally and rotationally excited. All energetically open channels have a significant population. Figure 5 shows vibrational distributions for a few energies. For low photodissociation energies, the maximum is located at $v = 0$, but with increasing excitation the maximum shifts to higher v values. At Ly α, the vibrational distributions have a maximum for $v = 3$. Figure 6 presents rotational distributions for a photon energy of 10.2 eV, corresponding to Ly α radiation, for different values of v. The rotational distributions are clearly inverted: the rotational levels with the highest probability are close to the highest open rotational state. In this respect, the rotational distributions resemble those of the OH(A) fragments,[6,8] although the population inversion is

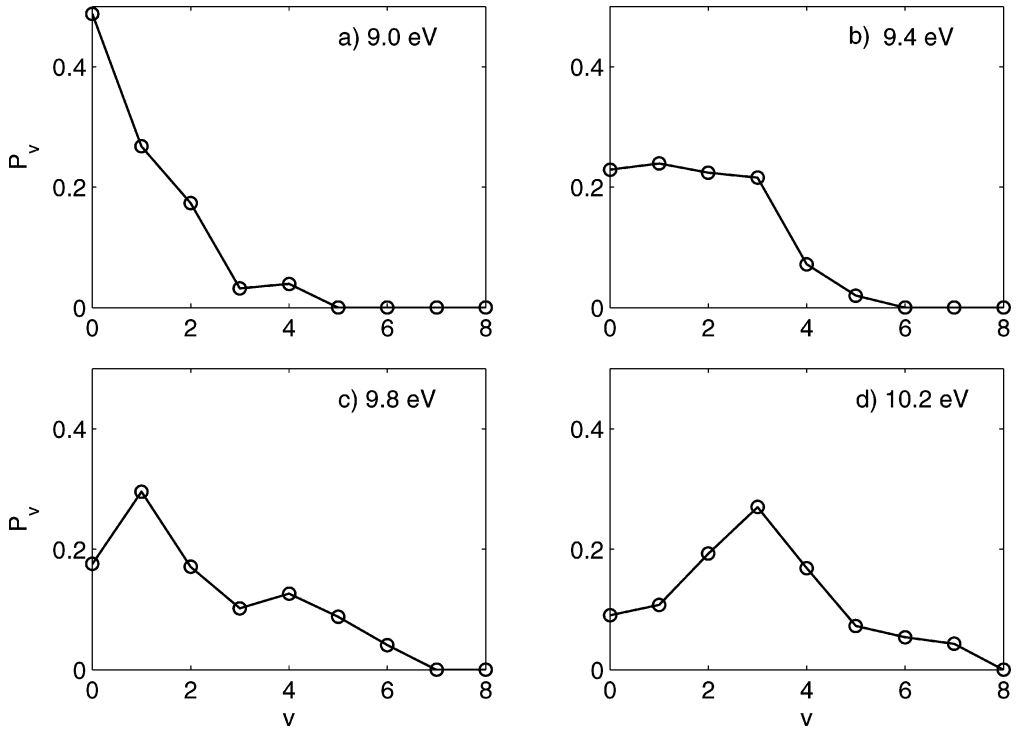

Figure 5. Vibrational distribution of the H_2 fragments at four different photon energies. P_v is the probability that the H_2 fragment is found in vibrational state v. The initial rotational state is 0_{00}.

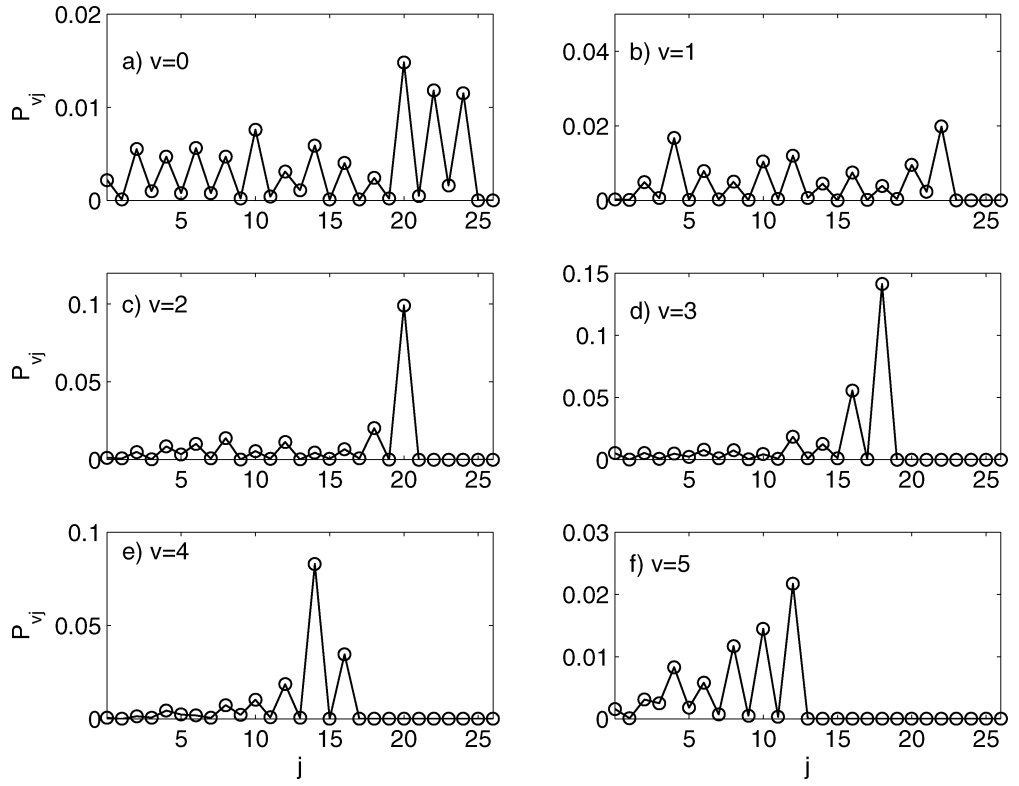

Figure 6. Rotational distributions of the H_2 fragment for a photon energy of 10.2 eV. Each panel shows the rotational distribution for specific vibrational state. P_{vj} is the probability that the H_2 fragment is found in vibrational state v and rotational state j. The initial rotational state is 0_{00}.

less extreme. The strong rotational excitation is the consequence of the indirect dissociation pathway for the $O(^1D) + H_2$ channel. Quasi-classical trajectory calculations[10] show that all H_2 fragments are formed after the molecule has rearranged to an OHH structure.

The rotational populations of the odd j levels is very low, but not exactly zero. It appears that all H_2 fragments with even j are formed on the $\tilde{X}$ and $\tilde{B}$ surfaces, while all products with odd j are formed on the $\tilde{A}$ surface. Thus, the small population of the odd j's is due to the Renner−Teller effect. Indeed, if the Renner−Teller coupling is switched-off, then the population of odd j levels is exactly zero.

That j is even for the $\tilde{X}$ and $\tilde{B}$ states and odd for the $\tilde{A}$ state can be explained by considering symmetry operators of the C_{2v}-

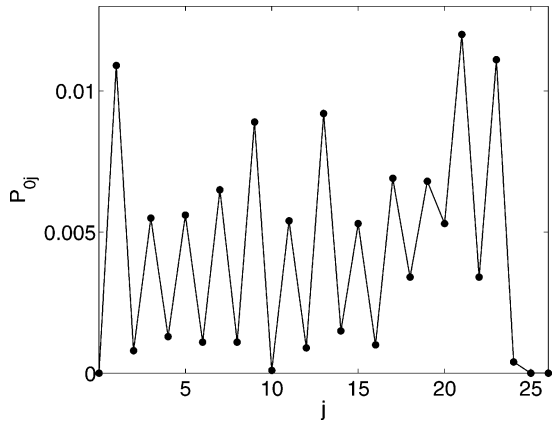

Figure 7. Rotational distributions of the $H_2(v = 0)$ fragments, for a photon energy of 10.2 eV, for the ground state of ortho water (1_{01}). P_{0j} is the probability that the H_2 fragment is found in vibrational state $v = 0$ and rotational state j.

TABLE 4. Effect of Symmetry Operators on the Basis Functions for AB_2 Molecules, for $A + B_2(R)$ and $A + B_2(r)$ Coordinate Systems

	$\tilde{P}_{j\Omega}(\gamma)$	$\Theta_{\Omega}^{JM\epsilon}(\omega)$ for *R*-emb.	$\Theta_{\Omega}^{JM\epsilon}(\omega)$ for *r*-emb.
(12)	$(-1)^{j+\Omega}$	$(-1)^{\Omega}$	$\epsilon(-1)^{J+\Omega}$
E^*	1	$\epsilon(-1)^{J}$	$\epsilon(-1)^{J}$
(12)*	$(-1)^{j+\Omega}$	$\epsilon(-1)^{J+\Omega}$	$(-1)^{\Omega}$

(M) molecular symmetry group.[19] The total wavefunction in the uncoupled roto-electronic representation (eq 2) is a sum over products of vibrational amplitudes, rotational basis functions, and electronic wavefunctions. Expanding the vibrational amplitudes $\chi_{\Omega n}(r, R, \gamma)$ of eq 2 in normalized associated Legendre polynomials $\tilde{P}_{j\Omega}(\gamma)$, the wavefunction can be written as

$$\Psi^{JMp} = \sum_{j\Omega n} f_{j\Omega n}(r, R)\tilde{P}_{j\Omega}(\gamma)\Theta_{\Omega}^{JM\epsilon_n}(\omega)|\psi_n^{\mathrm{el}}\rangle \qquad (17)$$

For *R*-embedding, *j* represents the rotational angular momentum of the H_2 fragment. In the wavepacket propagation, we employ the coupled roto-electronic representation (eq 6) for *r*-embedding, but to extract the rovibrational distributions of the H_2 fragments, the wavefunction is transformed to the form of eq 17 for *R* embedding. The symmetry properties of the various basis functions are discussed in the Appendix. Para water in the ground state (0_{00}) has symmetry species A_1. Since the dipole operator transforms as A_2,[19] the total wavefunction after excitation has symmetry species A_2. The $\tilde{X}$ and $\tilde{B}$ electronic wavefunctions transform as A_1. Thus, the product of the vibrational and rotational wavefunctions for the $\tilde{X}$ and $\tilde{B}$ states should transform as A_2. Table 4 of the Appendix shows that for *R*-embedding the product $\tilde{P}_{j\Omega}\Theta_{\Omega}^{JM\epsilon}(\omega)$ has A_2 symmetry if *j* is even and if $\epsilon = -(-1)^J$. All fragments formed on the $\tilde{X}$ and $\tilde{B}$ surfaces have therefore even *j*. Similar arguments explain why the fragments formed via the $\tilde{A}$ state, which transforms as B_1, all have odd *j*.

The previous discussion concerned water in the initial rotational state 0_{00}, which is the lowest rotational state of para water. For all rotational levels of para water (A_1 or A_2 levels), the H_2 fragments formed on the $\tilde{X}$ and $\tilde{B}$ surfaces have even *j*, and those formed via the $\tilde{A}$ state have odd *j*. Because most fragments are formed on the $\tilde{B}$ surface, even rotational levels are preferred for para water. For ortho water (B_1 or B_2 levels), the role of even and odd rotational levels is reversed: now the odd rotational levels are preferred. Figure 7 presents the rotational distribution for the ground state of ortho water, for photodissociation at Ly α. The rotational distribution is similar to the rotational distribution for para water, but now the odd *j* levels are preferred. However, the preference for odd *j* is less strong than the preference for even *j* in the case of para water. The reason is the increase of the Renner−Teller coupling due to the rotational excitation.

For higher excited rotational states, the preference for even or odd rotational levels is even weaker, due to the stronger Renner−Teller interaction. However, because most of the hydrogen fragments are formed via the $\tilde{B}$ state, a preference for a even or odd is still clearly visible even for the highly excited rotational states. Since the statistical weight for ortho water is three times that of para water, it can be expected that for thermally averaged water molecules the H_2 fragments are preferentially formed in odd rotational levels.

VI. Conclusion

We have presented absolute cross sections for the $O(^1D) + H_2$ dissociation channel, based on accurate quantum mechanical calculations including non-adiabatic effects. For Ly α photodissociation, the branching ratio for this channel was found to be 10% and nearly independent of the initial rotational state. This result is in good agreement with experiment.[1] Presented are also the rovibrational distributions of the H_2 fragments. The strong rotational and vibrational excitation is consistent with observations of cometary atmospheres.[11] However, the H_2 fragments produced in the photodissociation of water have never been observed directly. We hope that the present work will inspire experimentalist to study the molecular hydrogen fragments, for example using photofragment imagining techniques.

Acknowledgment. The work is financially supported by the Nederlandse Organisatie voor Wetenschappelijk Onderzoek (NWO).

Note Added in Proof. The accuracy of the H atom quantum yield reported by Yi et al.[18] (1.39) has been questioned by Sharma and Vatsa.[20]

Appendix

Symmetry of the Wavefunction for AB_2 Molecules. The discussion in section II was general. The only symmetry element common to all triatomic molecules in the inversion E^*, which we exploited by labeling the wavefunctions with the parity *p*. Molecules of the type AB_2 have additional symmetry operators. The effect of the additional symmetry can be seen in the rotational distributions of the B_2 fragment. The aim of this section is to determine the effect of the symmetry operators of the $C_{2v}(M)$ molecular symmetry group[19] on the basis functions used to represent the wavefunction. The following discussion assumes than an $A+B_2$ coordinate system is employed.

The symmetry operators can be decomposed in three terms:[19] $O = O_{\mathrm{vibronic}}O_{\mathrm{rot}}O_{\mathrm{nuclear\ spin}}$. The vibronic term only transforms the vibrational displacement from the equilibrium geometry and the electronic coordinates. The rotational term rotates the molecular frame. The nuclear spin term is not relevant for the present discussion, and it will be ignored in the following.

The molecular frame *xyz* for Jacobi coordinate systems is defined as follows. The *z* axis is parallel to the **r** or **R** vectors, depending on the embedding. The molecule lies in the *xz* plane: the *y*-axis is perpendicular to the molecular plane. For *R* embedding[19]

$$(12) = C_{2z}R_z^{\pi}, \quad E^* = \sigma_{xz}R_y^{\pi}, \quad (12)^* = \sigma_{yz}R_x^{\pi} \quad (R \text{ emb.}) \tag{18}$$

The vibronic operators C_{2z}, σ_{xz}, and σ_{yz} are the usual point group operators acting on the vibronic coordinates, and R_i^{π} is a rotation over π around the molecular fixed axes i. For r-embedding, interchange z and x in eq 18. By using eq 18, the effect of the symmetry operators on the vibrational and rotational basis functions can be derived straightforwardly. Table 4 shows the effect of the symmetry operators on the basis functions $\tilde{P}_{j\Omega}(\gamma)$ and $\Theta_{\Omega}^{JM\epsilon_n}(\omega)$.

The electronic wavefunction ψ_n^{el} depends on both nuclear and electronic coordinates. We can write $\psi_n^{\text{el}} = \psi_n^{\text{el}}(q, Q)$, where q and Q denote electronic and nuclear coordinates, respectively. Consider first the special case $Q = Q^*$, where Q^* is a reference geometry where the molecule has C_{2v} point group symmetry (equal AB bond lengths). The point Q^* is invariant with respect to operators O_{vibronic}. Only the electronic coordinates are changed. The electronic state $\psi_n^{\text{el}}(q, Q^*)$ transforms as one of the irreducible representations of the C_{2v} point group (A_1, B_1, B_2, and A_2). The symmetry species of $\psi_n^{\text{el}}(q, Q^*)$ can be obtained by inspecting the electronic wavefunction. We will now assume that the electronic wavefunction $\psi_n^{\text{el}}(q, Q)$ smoothly correlates with the $\psi_n^{\text{el}}(q, Q^*)$ state, and that the phase of the wavefunction is continuous. Then, the effect of the operator O_{vibronic} on the wavefunction $\psi_n^{\text{el}}(q, Q)$ is the same as the effect of the corresponding point group operator on the wavefunction $\psi^n(q, Q^*)$.

For example, consider an A″ electronic state, that correlates with a B_1 state at C_{2v} point group symmetries. Then, we have in R-embedding $C_{2z}\psi_n^{\text{el}}(q, Q) = -\psi_n^{\text{el}}(q, Q)$. If, on the other hand, the A″ correlates with an A_2 state, then $C_{2z}\psi_n^{\text{el}}(q, Q) = +\psi_n^{\text{el}}(q, Q)$.

References and Notes

(1) Slanger, T. G.; Black, G. *J. Chem. Phys.* **1982**, *77*, 2432.
(2) Mordaunt, D. H.; Ashfold, M. N. R.; Dixon, R. N. *J. Chem. Phys.* **1994**, *100*, 7360.
(3) Harich, S. A.; Yang, X. F.; Yang, X.; van Harrevelt, R.; van Hemert, M. C. *Phys. Rev. Lett.* **2001**, *87*, 263001.
(4) Hwang, D. W.; Yang, X. F.; Harich, S.; Lin, J. J.; Yang, X. *J. Chem. Phys.* **1999**, *110*, 4123.
(5) Dixon, R. N.; Hwang, D. W.; Yang, X. F.; Harich, S.; Lin, J. J.; Yang, X. *Science* **1999**, *285*, 1249.
(6) Harich, S. A.; Hwang, D. W. H.; Yang, X.; Lin, J. J.; Yang, X.; Dixon, R. N. *J. Chem. Phys.* **2000**, *113*, 10073.
(7) Harich, S. A.; Yang, X.; Yang, X.; Dixon, R. N. *Phys. Rev. Lett.* **2001**, *87*, 253201.
(8) Fillion, J. H.; van Harrevelt, R.; Ruiz, J.; Castillejo, M.; Zanganeh, A. H.; Lemaire, J. L.; van Hemert, M. C.; Rostas, F. *J. Phys. Chem. A* **2001**, *105*, 11414.
(9) van Harrevelt, R.; van Hemert, M. C. *J. Chem. Phys.* **2000**, *112*, 5787.
(10) van Harrevelt, R.; van Hemert, M. C.; Schatz, G. C. *J. Phys. Chem. A* **2001**, *105*, 11480.
(11) Liu, X.; Shemansky, D. E.; Hallett, J. T.; Weaver, H. A. *Astrophys. J. Suppl. Series* **2007**, *169*, 458.
(12) Dobbyn, A. J.; Knowles, P. J. *Mol. Phys.* **1997**, *91*, 1107.
(13) Petrongolo, C. *J. Chem. Phys.* **1988**, *89*, 1297.
(14) Zare, R. N. *Angular momentum: Understanding Spatial Aspects in Physics and Chemistry;* Wiley: New York, 1988.
(15) Tennyson, J.; Sutcliffe, B. T. *J. Mol. Spectrosc.* **1983**, *101*, 71.
(16) van Harrevelt, R.; van Hemert, M. C. *J. Chem. Phys.* **2000**, *112*, 5777.
(17) van Harrevelt, R.; van Hemert, M. C. *Chem. Phys. Lett.* **2003**, *370*, 706.
(18) Yi, W.; Park, J.; Lee, J. *Chem. Phys. Lett.* **2007**, *439*, 46.
(19) Bunker, P. R.; Jensen, P. *Molecular Symmetry and Spectroscopy*; NRC Research Press: Ottawa, 1998.
(20) Sharma, P.; Vatsa, R. K. *Chem. Phys. Lett.* **2007**, *446*, 401.